Journal of Ovonic Research Vol. 10, No. 6, November - December 2014, p. 247 - 256

STUDY OF ANNEALING EFFECTS ON THE PHYSICAL PROPERTIES OF EVAPORATED SnS THIN FILMS FOR PHOTOVOLTAIC APPLICATIONS

G.H. TARIQ[a,b*], K. HUTCHINGS[b], GHULAM ASGHAR[c], D.W. LANE[b], M. ANIS-UR-REHMAN[a]
[a]*Department of Physics, COMSATS Institute of Information Technology, Islamabad, Pakistan*
[b]*Department of Materials Science and Radiation Group, Cranfield University, Defence Academy of the UK, Shrivenham SN6 8LA, UK*
[c]*Department of Physics, The University of Poonch, Rawalakot , Azad Jammu & Kashmir, Pakistan*

Tin Sulphide (SnS) thin films have been deposited on glass slides by thermal evaporation using SnS powder. The improvements in the structural and optical properties of SnS thin films on annealing at different temperatures (200°C, 300°C, 400°C, and 500°C) in vacuum for one hour are presented in this work. The thin films annealed at 500°C were decomposed, which limits the annealing temperature below than 500°C. X-ray diffraction characterization showed an intensive peak at 31.8° originating from *(111)* reflection. Ellipsometry measurements were done for optical studies and optical absorption coefficient for as-deposited films was 2.02 x10^4 increased to 4.90 x10^4 $(cm)^{-1}$ for films annealed to 300°C for incident photon energies 1.55eV, and direct band gap of 1.90 eV was indicated.

(Received October 26, 2014; Accepted December 3, 2014)

Keywords: SnS, Thermal evaporation, Ceramic crucible, Absorption coefficient, Band gap

1. Introduction

In the existing energy crisis due to depletion of energy resources and increase in demand for energy, the world is searching for a possible alternative to hydrocarbons. Solar cells have taken an interest of researchers. The solar cells can provide a source of thermal and electrical energy. Research into cheaper and more efficient solar cells has been underway for several decades and researchers are investigating the properties of different thin film materials for solar cells photovoltaics [1-4].

Tin sulphide (SnS) is an IV-VI binary semiconductor compound whose constituent elements Tin (Sn) and Sulphur (S) are abundant in nature. SnS in its orthorhombic crystalline structure has direct and indirect band gap values between 1.3–1.5 eV and 1.0–1.1 eV, respectively and has p-type conductivity. It has higher absorption coefficient (~10^5 cm^{-1}) compare to other materials like GaAs and CdTe. These properties make it a better alternative absorber material for photovoltaic applications.

Different deposition techniques such as chemical spray paralysis (CSP) [5], vacuum evaporation [6-8], chemical bath deposition (CBD) [9-10], pulsed electrochemical deposition [11], and RF sputtering [12] have been used for the fabrication of SnS thin films. Recently investigations on new photovoltaic materials have been considerable interest and researchers are investigating for understanding and engineering the properties of SnS thin films for photovoltaic applications [5-8, 13]. To improve efficiency of these devices better understanding of physical properties such as structural, electrical and optical properties is required. In our present work we have studied the effects of annealing on the physical properties of SnS thin films deposited by

* Corresponding author: g.hasnain@yahoo.com

thermal evaporation. Our goal is to develop better growth approach and understanding of this new non-toxic material for the fabrication of low cost solar cells. Generally, to improve structural, electrical and optical properties post-deposition annealing is used. Improvement in these properties plays a major role in enhancing the device efficiency. Our present work is particularly concerned with the study of influence of annealing temperature on structural and optical properties of SnS thin films deposited by thermal evaporation.

2. Experimental details

2.1. Thin films deposition

SnS thin films were deposited from powder material via thermal evaporation technique onto clean glass substrates held at the chamber ambient temperature. The deposition process was carried out at a pressure of ~10^{-5} mbar using a high vacuum coating unit. During deposition the film thickness as well as the deposition rate was controlled by means of thickness monitor having quartz crystal, other important controlled parameters were the source to substrate distance, and source temperature. The samples preparation process begins with the substrate cleaning, which was done in three steps; (i) the substrates were cleaned using soft electric brush using a 5% solution of laboratory detergent Decon 90 (Decon Laboratories Limited, Hove, UK) and distilled water, (ii) in the second step with ultrasonic bath using isopropyl alcohol, and (iii) finally cleaning of substrates was completed with drying in N_2 flow. The substrates were placed on the substrate holder and the distance between the source and the substrate was kept same for all depositions at approximately 21cm. SnS powder was evaporated in the ceramic crucible that was placed in molybdenum (Mo) cylindrical shaped wire element for heating. The 99.995% pure SnS powder was obtained from Kurt J. Lesker Company. During deposition the source temperature was kept same for all samples by controlling the source current. The coating system was evacuated with base vacuum of $3x10^{-6}$ mbar by an oil diffusion pump with a liquid nitrogen trap and a rotary pump. After deposition, prepared thin films were encapsulated in evacuated Pyrex glass ampoules having pressure around 10^{-2} Torr and annealed at different annealing temperatures (Ta) as-deposited, 200°C, 300°C, and 400°C for 1 hour.

2.2. Characterization of thin films

Both the as-deposited and annealed thin films of SnS used for study have same thickness, adherent to the glass substrate and dark brown in appearance. These prepared samples were structurally analyzed by XRD for phase identification, grain size/morphology, lattice parameter, microstrain and dislocation density. Also Raman spectroscopy was used for phase confirmation. Energy dispersive X-ray (EDX) attached to SEM was carried out for chemical compositional analysis and further this analysis was used to qualitatively measure the sample stoichiometry. Optical analysis for transmission studies and to find optical constants like absorption coefficient and band gap was done by using ellipsometry.

3. Results and Discussion

3.1. Crystalline structure analysis

X-ray diffraction (XRD) measurement provides insight into the structural properties crystal analysis of the as deposited and annealed SnS films. The structural analysis of these films was performed using X-ray diffractometer (XRD) with a CuKα radiations (λ=1.5406 *Å*) with 2θ ranging from 21° to 56°. XRD patterns of these as deposited and annealed thin films showed evidence of their polycrystalline nature and is presented in Fig 1. Also these SnS thin films exhibit orthorhombic crystal structure with preferential orientation along the *(111)* direction and this peak fits well with JCPDS data card: 14-620. The intensity of this peak became greater and sharper with

increasing the annealing temperature. This results a decrease in FWHM and an increase in crystallite size with increasing annealing temperature. While some additional small peaks were grown in the samples annealed at 400°C temperature. This observed growth in peak's intensity is the evidence of dependence of prepared samples crystallinity on annealing temperature. It can be said that the un-annealed/as-deposited thin film was poor polycrystalline and nearly amorphous, while turned to be crystalline after annealing. It was observed that the thin film annealed at 400°C has some additional diffraction peaks; same crystalline structure was also identified by other researchers [6].

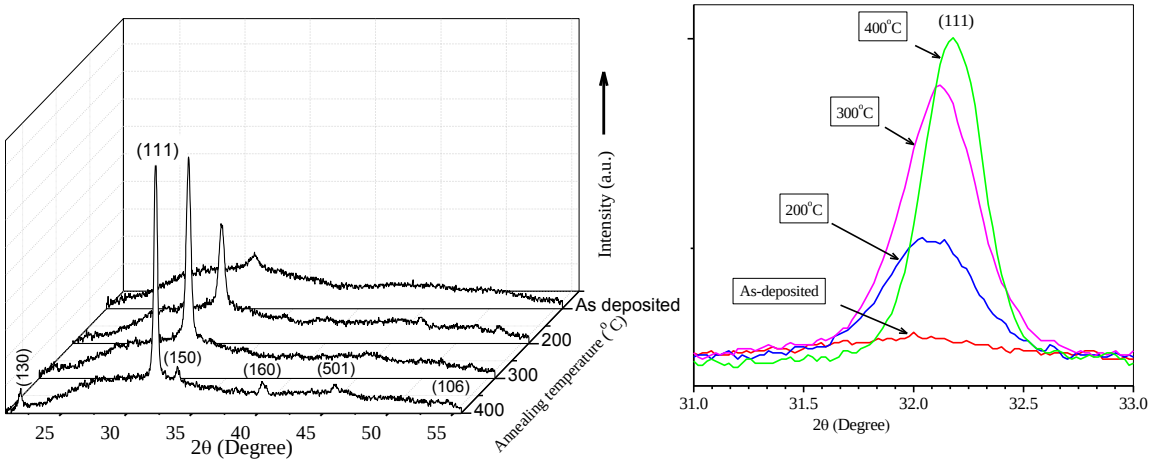

Fig.1. XRD patterns for annealed and as-deposited SnS thin film

We obtained that the post deposition annealing caused an increase in the intensity of the main reflections with increasing temperature and so the layers becoming more oriented and perhaps more crystalline. On the other hand, for (*111*) plane the full width at half maximum (FWHM) decreases with increasing the annealing temperature, indicating an increase of the grain size with increasing the annealing temperature as shown in Fig 2.

3.1.1. Crystallite size /morphology

From the obtained X-ray diffraction data the mean crystallite size of the preferred *(111)* orientation was calculated by using Debye–Scherrer's formula [14],

$$G = {0.9\lambda}/{(\beta cos\theta)} \quad (1)$$

where λ is the wavelength of the X-rays used for measurements; β is the full width half maximum of the corresponding peak and θ is the Bragg angle. The average grain size was affected due to vacuum annealing and was increased from $21nm$ to $29nm$ after annealing. This was observed that change in grain size is annealing temperature dependent. This effect may be attributed to the rearrangement of atoms and recrystallisation of the films during the annealing process.
The number of crystallites per unit area (*N*) was calculated by using Eq. (2) [15] and was found to be decreased 3.50×10^{16} m^{-2} to 1.39×10^{16} m^{-2} on increasing annealing temperature up to 400°C. This decreasing trend can be attributed to the increasing size of crystallites.

$$N = {t}/{G^3}\ (per\ unit\ area) \quad (2)$$

where 't' is the film thickness, and 'G' is the grain size.

3.1.2. Dislocation Density and Microstrains

As a thin film solar cell is a hetrojunction device, so it is necessary to reduce the dislocation density and microstrain and to improve uniformity of the SnS thin films' surface. The value of the dislocation density (δ) which gives the number of defects in the film was calculated with the help of Williamson and Smallman's equation [16],

$$\delta = \frac{1}{D^2} \tag{3}$$

Microstrains were calculated by the following relation [17],

$$\varepsilon = \frac{\beta cos\theta}{4} \tag{4}$$

The obtained values of crystallite size, dislocation density, microstrain and number of crystallites per unit area of SnS thin films are presented in Fig 2 and table 1.

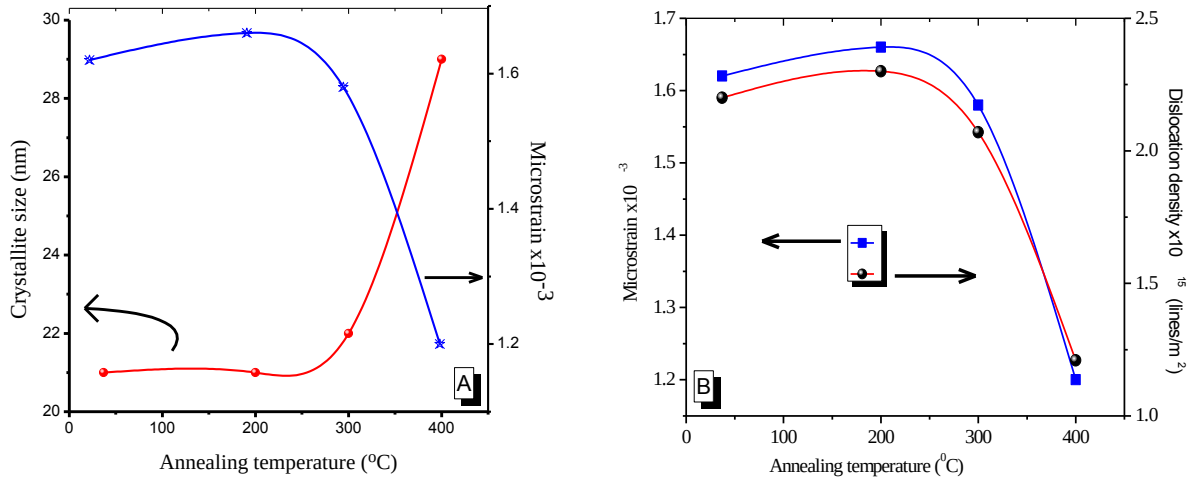

Fig.2. Annealing temperature dependences of crystallite size, microstrain and dislocation density

Table 1: Crystallite size, dislocation density, microstrains and number of crystallites per unit area of SnS thin films

Sample	G (nm)	δ $\times (10)^{15}(lines\ m^{-2})$	ε $\times (10)^{-3}$	N $\times (10^{16})\ m^{-2}$
As deposited	21	2.20	1.62	3.50
200°C	21	2.30	1.66	3.50
300°C	22	2.07	1.58	3.21
400°C	29	1.21	1.20	1.39

Further texture coefficient is an important factor for exact structural characterization of a material and this is one of the basic structure parameters in all polycrystalline materials. Texture coefficient was determined in order to find preferential orientation of crystallites in deposited polycrystalline SnS thin films after annealing. Using the following equation [18] texture coefficient was calculated from the x-ray diffraction results:

$$T_c(hkl) = \frac{I(hkl)/I_0(hkl)}{N^{-1}\sum_n I(hkl)/I_0(hkl)} \tag{5}$$

Where, $T_c(hkl)$ is the texture coefficient of (hkl) plane, $I(hkl)$ is the intensity measured for (hkl) plane, $I(hkl)$ is the intensity of (hkl) plane taken from standard data in JCPDS data card fitting in the x-ray diffraction pattern of material, n is the diffraction peak number and N is the total reflection number. For a film to have a preferential orientation at any (hkl) plane, the texture coefficient must be at least one [18]. The values of the texture coefficient for all of the planes of SnS thin films were calculated. From these calculated values of the texture coefficient, it was found that the preferential orientation was along *(111)* plane. This denotes that the number of grains along this plane is more than the other planes.

3.2. Raman Analysis

Raman scattering measurements were carried out at room temperature on prepared and annealed SnS gradient layers. The 24 vibrational modes for orthorhombic structure of SnS are represented as [19]:

$$\Gamma = 4A_g + 2B_{1g} + 4B_{2g} + 2B_{3g} + 2A_u + 4B_{1u} + 2B_{2u} + 4B_{3u} \quad (6)$$

SnS has 21 optical phonons including 12 Raman active modes ($4A_g + 2B_{1g} + 4B_{2g} and\ 2B_{3g}$), seven infrared active modes ($3B_{1u} + 1B_{2u} and\ 3B_{3u}$) and two inactive ($2A_u$) [19]. The Raman spectra of the nanostructured SnS thin films exhibits a strong and large peak located at 225 cm^{-1} and other at 307 cm^{-1}. The obtained Raman spectra of the SnS thin films annealed at different temperatures is presented in Fig 3. The main change observed in the Raman spectra of all the SnS films due to annealing is that the intensity of the 307 cm^{-1} shoulder increases and the intensity of the 225 cm^{-1} increased for films annealed to 300°C, while decreased for film annealed to 400°C.

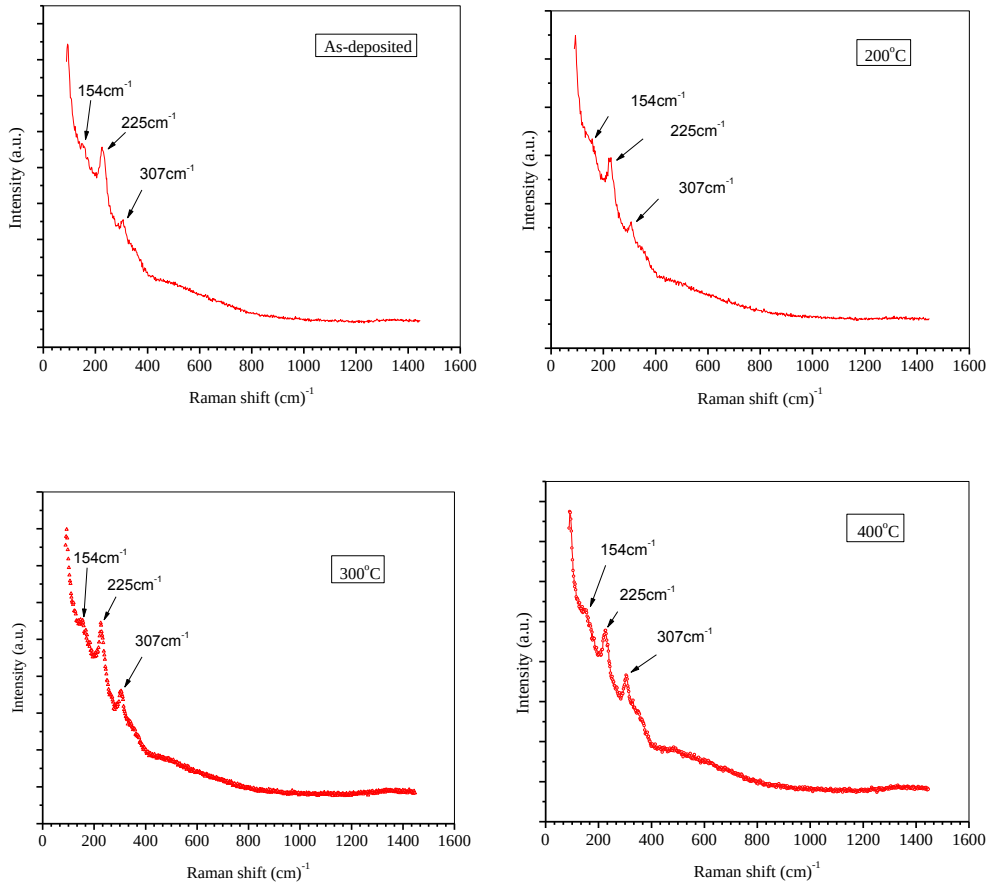

Fig.3. Raman spectra of the SnS thin films annealed at different temperatures

3.3. Compositional Analysis

Elemental composition of SnS thin films was determined by using a computer controlled digital scanning electron microscope attached with the EDX system. The variation of S to Sn atomic ratio of as-deposited and annealed SnS films is shown in figure. The S to Sn atomic % ratio decreased from 1.53 to 1.27 on increasing Ta from as-deposited to 400°C. The same behavior was also observed by other researchers [20] and deficiency of sulfur at higher Ta was attributed due to high vapour pressure of sulfur. The Dependence of S/Sn % and number of crystallites on annealing temperature is given in the Fig 4.

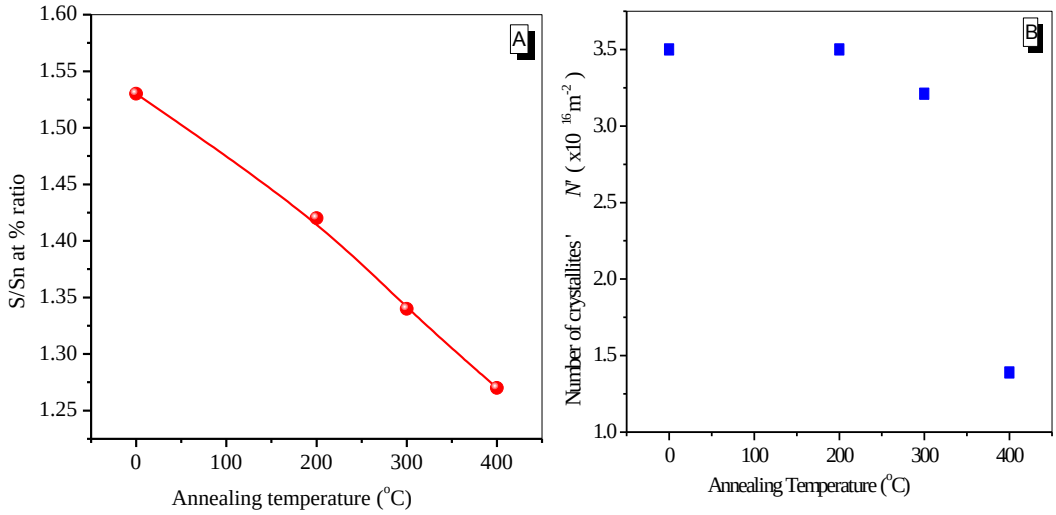

Fig.4. Dependence of S/Sn % and number of crystallites on annealing temperature

3.4 Optical studies

3.4.1. Transmission Analysis

The optical transmission spectra of prepared films were acquired with an ellipsometer operated in air at room temperature and using normal incidence in 200nm-1700nm spectral range. For the interference minima and maxima with normal incidence of optical radiation for certain film the wavelength satisfy the following relation [21],

$$2n.d = m.\lambda \tag{7}$$

Where 'm' is an integer number and semi integer number for interference maxima and minima respectively. Optical transmission spectra were obtained for as-deposited and annealed SnS films and dependency of transmission on annealing temperature was studied. The % optical transmission of the as-deposited and annealed SnS films is displayed in Fig 5 (A). There was no light transmission for wavelengths from 200 to 500 nm for as-deposited films and films annealed at 200°C, while to 600nm for films annealed at 300°C and 400°C. In the weak absorption region better interference patterns were observed for annealed films, which confirmed the formation of uniform and smooth films and indicated that the air/layer and layer/glass interfaces are smooth [22]. The blue shift observed in all the annealed thin films may be due to the creation of new bonds. The wave like nature is considered occurs from interference fringes caused by the substrate-film and film-air interference [10]. Fig 5 (A) showed that the post-deposition annealing treatments influence the optical properties of these SnS films intensely. From these transmission spectra the observed average optical transmittance found to be dependent upon annealing temperature. For the as-deposited thin films transmission is about 17 % at 650 nm which reduces to about 3% after annealing these thin films in the vacuum at 400°C.

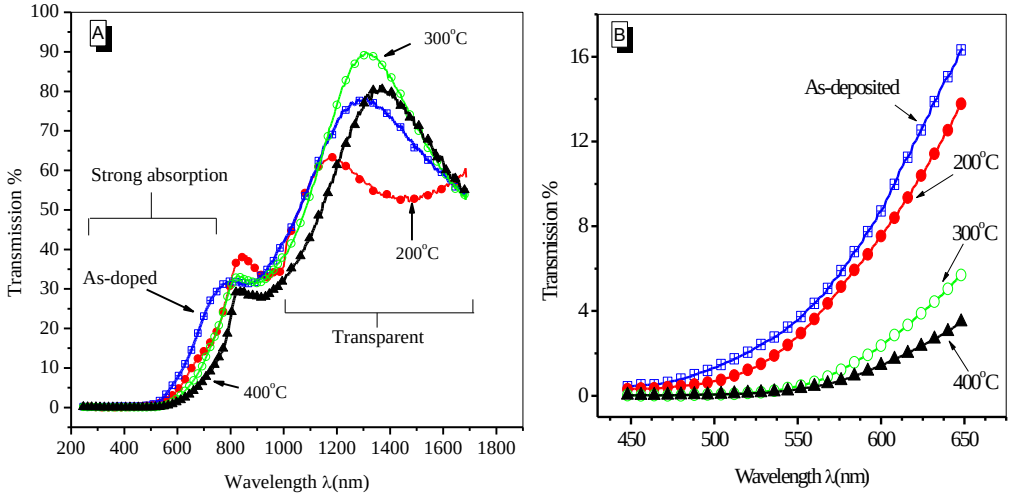

Fig.5. Transmission spectra of samples depending upon annealing temperature

The effect of vacuum annealing on optical studies of SnS films in the present work showed a shift of the fundamental optical absorption edge towards the UV from 450 to 650 nm may be due to an increase in the concentration of free carriers shown in Fig 5 (B). This may be due to improvement in crystallinity.

3.4.2. Absorption coefficient and energy band gap

The optical absorption coefficient "α" of SnS thin films was calculated using the Lambert's formula using the % transmission (%T) value measured for a particular wavelength and film thickness (t) using the relation [23, 24]

$$\alpha = \frac{-\ln(\%T/100)}{t} \tag{8}$$

For this equation it is assumed that the reflection in the short wavelength region is negligible. The observed variation of absorption coefficient for these as-deposited and vacuum annealed SnS films is shown in Fig 6. The results showed that the absorption coefficient of as-deposited SnS films was increased from 2.02 x10^4 to 4.90 x10^4 $(cm)^{-1}$ with annealing to 300°C and was decreased on further higher annealing to 400°C, for incident light with 800nm wavelength. The absorption coefficient of annealed SnS films was also observed >3 x10^4 $(cm)^{-1}$ by other researchers [10, 25].

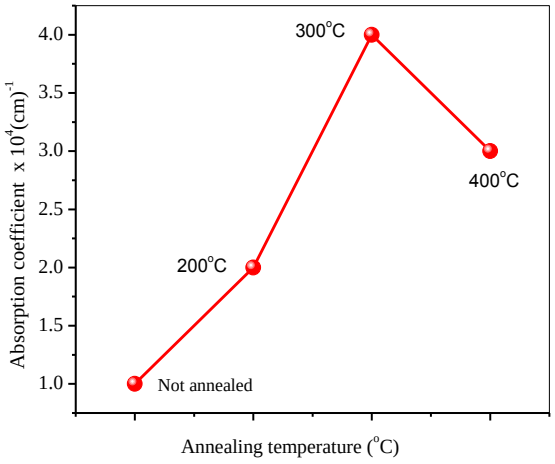

Fig.6. Absorption coefficient Vs annealing temperature

In polycrystalline materials direct and indirect transitions depend on band structure of the material. From the obtained optical absorption spectra the value of band gap can be obtained by using Tauc relation [26],

$$\alpha h\nu = B\left(h\nu - E_g\right)^n \qquad (9)$$

where , B is a constant, α is the absorption coefficient, ν is the frequency of incident light, h is Plank's constant and n has the values of 1/2, 2, 3/2 and 3 depending for allowed direct, allowed indirect, forbidden direct and forbidden indirect transitions, respectively. The optical band gap (E_g) of these as-deposited and annealed SnS films was determined using $(\alpha h\nu)^2$ versus incident photon energy ($h\nu$) plots and by extrapolating the plots onto α = 0, the x-intercept gave the value of band gap.

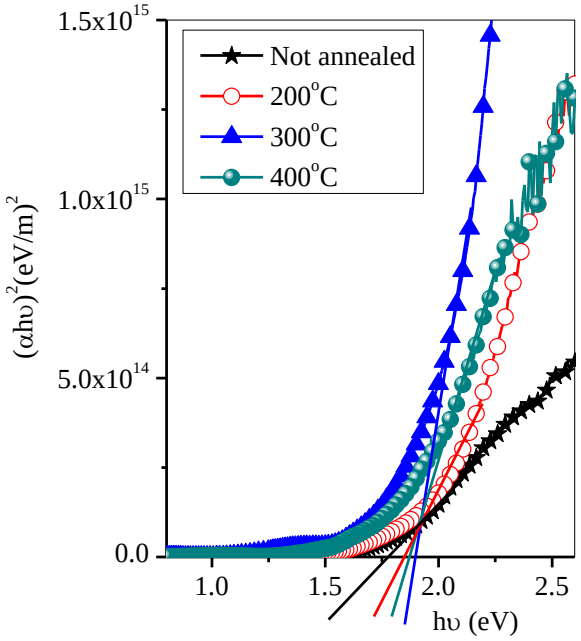

Fig.7. Determination of the optical gaps in terms of Tauc's relation

The obtained optical band gap of the as-deposited films was 1.78eV and increased to 1.90eV for the films at 300°C. The band gap determined for films annealed at 300°C was 1.90 eV which was decreased to 1.85 eV for films annealed further at 400°C. This decrease in the band gap may attribute to the structure of thin films at 400°C. The band gap values of as-deposited and annealed at higher annealing temperatures are higher than the range of 1.30–1.83 eV which is the value of direct energy band gap of SnS thin Films [10]. The observed increase in direct band gap for the annealed films can be explained with their crystalline structure and increased grain size of films, as revealed by XRD patterns and explained also by other researchers [27]. These obtained results illustrated the similarity to other's works. These detected differences in the E_g values can be attributed mainly to the film growth conditions during this work, which lead to produce different grain sizes and lattice parameters. Therefore, the band gap of these films is slightly higher related to bulk SnS. Different obtained optical parameters are given in table 2 and presented in Fig 8.

Table 2: Optical parameters of as-deposited and annealed films

Annealing	Band gap (eV)	α $(cm)^{-1}$ at 800nm
As-deposited	1.78	2.02 $x10^4$
200˚C	1.85	2.68 $x10^4$
300˚C	1.90	4.90 $x10^4$
400˚C	1.87	3.06$x10^4$

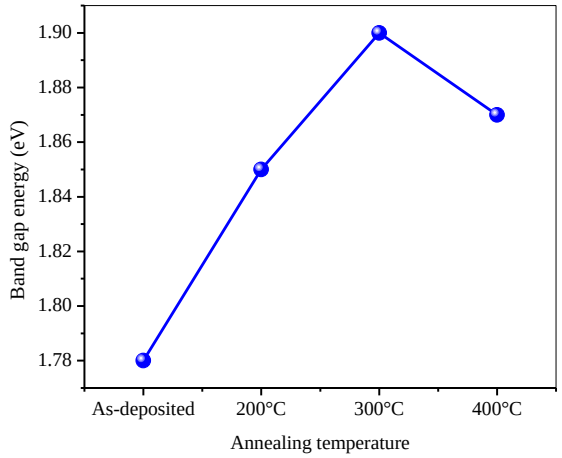

Fig.8. Dependency of band gap energy on annealing temperature

4. Conclusions

In this paper we have reported the influence of annealing temperature on prepared SnS films by thermal evaporation and annealed at various temperatures range as-deposited, 200°C, 300°C and 400°C in vacuum environment by encapsulating in Pyrex glass ampoules. Both XRD and Raman analyses of as-deposited and annealed SnS thin films indicated no degradation of the film structure and showed improvement of crystalline structure. Annealing at 300^{o}C of thermally evaporated SnS thin films results an absorption coefficient of 3.06x10^4 cm^{-1} and optical energy band gap of 1.90 eV. On the basis of these results, it can be accepted that thin layers of SnS absorb much of the radiation and that they are adequate to be used as an absorber layer in photovoltaic devices like thin film solar cells.

Acknowledgments

This study was completed by financial support of Higher Education Commission Pakistan, by providing funds for the abroad visit to one of the authors (G. H. Tariq) through 'International Research Support Initiative Programme (IRSIP)' and 'Indigenous 5000 Scholarship Programme' and was also supported by the EPSRC funded SUPERGEN Project, Photovoltaic Materials for the 20th Century (EP/F029624/2).We are thankful to Mike Sallwood at Rutherford lab who managed the equipment for deposition of samples and Richard Hall who facilitated by encapsulating samples in evacuated Pyrex glass ampoules for annealing. We are grateful to Jon Painter for providing EDX characterization facility. One of the authors (G. H. Tariq) would like to thanks the department of education, Govt. of the Punjab, Pakistan for granting him a leave for this work.

References

[1] J. B. Li, V. Chawla, and B. M. Clemens, (2012), Adv. Mater. **24,** 720 (2012)
[2] P. P. Choi, O. C. Miredin, and R. Wuerz, Surf. Interface Anal. **44,** 1386 (2012).

[3] J. J. Scragg, P. J. Dale, D. Colombara, and L. M. Peter, ChemPhysChem. **13,** 3035 (2012).
[4] L. Grenet, S. Bernardi, D. Kohen, C. Lepoittevin, S. Noel, N. Karst, A. Brioude, S. Perraud, H. Mariette, Solar Energy Mater. & Solar Cells **101,** 11 (2012).
[5] T. H. Sajeesh, A. S. Cherian, C. S. Kartha and K. P. Vijayakumar; Energy Procedia **15**, 325 (2012).
[6] O. E. Ogah, K. R. Reddy, G. Zoppi, I. Forbes and R. W. Miles, Thin Solid Films **519**, 7425 (2011).
[7] P. A. Nwofe, K. T. R. Reddy, G. Sreedevi, J. K. Tan, I. Forbes, R. W. Miles, Energy Procedia **15**, 354 (2012).
[8] P. A. Nwofe, K. T. R. Reddy, J. K. Tan, I. Forbes and R. W. Miles, Physics Procedia **25,** 150 (2012).
[9] C. Gao and H. Shen, Thin Solid Films **520**, 3523–3527 (2012).
[10] E. Guneri, C. Ulutas, F. Kirmizigul, G. Altindemir, F. Gode, C. Gumus, Appl. Sur. Sc. **257**, 1189 (2010).
[11] M. Gunasekaran and M. Ichimura, Solar Ener. Mater. & Solar Cells **91,** 774–778 (2007).
[12] K. Hartman , J. L. Johnson , M. I. Bertoni , D. Recht , M. J. Aziz, M. A. Scarpulla , T. Buonassisi, Thin Solid Films **519**, 7421 (2011).
[13] T. H. Sajeesh, K. B. Jinesh, M. Rao, C. S. Kartha, and K. P. Vijayakumar, Phys. Status Solidi A **209,** (7) 1274 (2012).
[14] B. D. Cullity, S. R. Stock, Elements of X-Ray Diffraction 3rd ed., Prentice Hall, New York (2001).
[15] M. Dhanam, P. K. Manoj and R. R. Prabhu, J.Cry. Growth **280**, 425 (2005).
[16] S. Lalitha, R. Sathyamoorthy, S. Senthilarasu, A. Subbarayan, K. Natarajan, Sol. Energy Mater. Sol. Cells **82**, 187 (2004).
[17] G. H. Tariq, N. A. Niaz, and M. Anis-ur-Rehman, Chalcogenide Lett. **11,** (9) 461 (2014).
[18] E. Guneri, C. Gumus, F. Mansur, and F. Kirmizigul, Optoelectron. Adv. Mater. Rapid Commun. **3**, 383 (2009).
[19] S. Sohila, M. Rajalakshmi, C. Ghosh, A. K. Arora and C. Muthamizhchelvan, J. Alloys Compounds **509,** 5843 (2011).
[20] M. Devika, K. T. Ramakrishna Reddy, N. Koteeswara Reddy, K. Ramesh, R. Ganesan, E. S. R. Gopal, K. R. Gunasekhar, J. Appl. Phys. **100**, 023518 (2006).
[21] H. A. Radi, and J. O. Rasmussen, "Principles of Physics: For Scientists and Engineers", Springer-Verlag, Berlin (2013).
[22] B. Zengir, M. Bayhan, and S. Kavasouglu, J. of Arts and sciences Sayt: **5**, (2006).
[23] S. Prabahar, M. Dhanam, J. of Crys. Growth **285**, 41 (2005).
[24] D. Sumangala, Devi Amma, V. K. Vaidyan, P. K. Manoj, Mater. Chem. Phys. **93,** 194 (2005).
[25] M. Devika, N. K. Reddy, K. Ramesh, K. R. Gunasekhar, E. S. R. Gopal and K. T. R. Reddy, Semicond. Sci. Technol. **21,** 1125 (2006).
[26] J. Tauc, R. Grigorovic, and A. Vancu, Phys. stat. sol. **15,** 627 (1966).
[27] M. R. Fadavieslam, N. Shahtahmasebi, M. Rezaee-Roknabadi and M. M. B. Ohagheghi, Phys. Scr. **84,** 035705 (2011).